Author Manuscript

Author Manuscript

Author Manuscript

Author Manuscript

HHS Public Access

Author manuscript

Colloids Surf B Biointerfaces. Author manuscript; available in PMC 2017 July 01.

Published in final edited form as:

Colloids Surf B Biointerfaces. 2016 July 01; 143: 156–167. doi:10.1016/j.colsurfb.2016.03.036.

Ultra-flexible nanocarriers for enhanced topical delivery of a highly lipophilic antioxidative molecule for skin cancer chemoprevention

Cedar H. A. Boakye[1], **Ketan Patel**[1], **Ravi Doddapaneni**[1], **Arvind Bagde**[1], **Nusrat Chowdhury**[1], **Stephen Safe**[2], and **Mandip Singh**[1,*]

[1]College of Pharmacy and Pharmaceutical Sciences, Florida A&M University, Tallahassee, FL 32307, USA

[2]Department of Veterinary Physiology and Pharmacology, Texas A&M University, TX 77843, USA.

Abstract

Purpose—In this study, we developed cationic ultra-flexible nanocarriers (UltraFLEX-Nano) to surmount the skin barrier structure and to potentiate the topical delivery of a highly lipophilic antioxidative diindolylmethane derivative (DIM-D) for the inhibition of UV-induced DNA damage and skin carcinogenesis.

Methods—UltraFLEX-Nano was prepared with 1,2-dipalmitoyl-*sn*-glycero-3-phosphocholine, 1,2-dioleoyl-3-trimethylammonium-propane, cholesterol and tween-80 by ethanolic injection method; was characterized by Differential Scanning Calorimetric (DSC), Fourier Transform Infrared (FT-IR) and Atomic Force Microscopic (phase-imaging) analyses and permeation studies were performed in dermatomed human skin. The efficacy of DIM-D-UltraFLEX-Nano for skin cancer chemoprevention was evaluated in UVB-induced skin cancer model *in vivo*.

Results—DIM-D-UltraFLEX-Nano formed a stable mono-dispersion (110.50±0.71nm) with >90% encapsulation of DIM-D that was supported by HPLC, DSC, FT-IR and AFM phase imaging. The blank formulation was non-toxic to human embryonic kidney cells. UltraFLEX-Nano was vastly deformable and highly permeable across the stratum corneum; there was significant ($p<0.01$) skin deposition of DIM-D for UltraFLEX-Nano that was superior to PEG solution (13.83-fold). DIM-D-UltraFLEX-Nano pretreatment delayed the onset of UVB-induced tumorigenesis (2 weeks) and reduced ($p<0.05$) the number of tumors observed in SKH-1 mice (3.33-fold), which was comparable to pretreatment with sunscreen (SPF30). Also, DIM-D-UltraFLEX-Nano caused decrease ($p<0.05$) in UV-induced DNA damage (8-hydroxydeoxyguanosine), skin inflammation (PCNA), epidermal hyperplasia (c-myc, CyclinD1),

[*]**Corresponding Author:** Mandip Singh, Professor and Section Leader, Pharmaceutics, 1520 S Martin Luther King Jr. Blvd, College of Pharmacy and Pharmaceutical Sciences, Florida A&M University, Tallahassee, FL 32307; Tel: (850) 561-2790; Fax: (850) 599-3813; mandip.sachdeva@gmail.com.

Publisher's Disclaimer: This is a PDF file of an unedited manuscript that has been accepted for publication. As a service to our customers we are providing this early version of the manuscript. The manuscript will undergo copyediting, typesetting, and review of the resulting proof before it is published in its final citable form. Please note that during the production process errors may be discovered which could affect the content, and all legal disclaimers that apply to the journal pertain.

Author Manuscript Author Manuscript Author Manuscript Author Manuscript

immunosuppression (IL10), cell survival (AKT), metastasis (Vimentin, MMP-9, TIMP1) but increase in apoptosis (p53 and p21).

Conclusion—UltraFLEX-Nano was efficient in enhancing the topical delivery of DIM-D. DIM-D-UltraFLEX-Nano was efficacious in delaying skin tumor incidence and multiplicity in SKH mice comparable to sunscreen (SPF30).

Graphical abstract

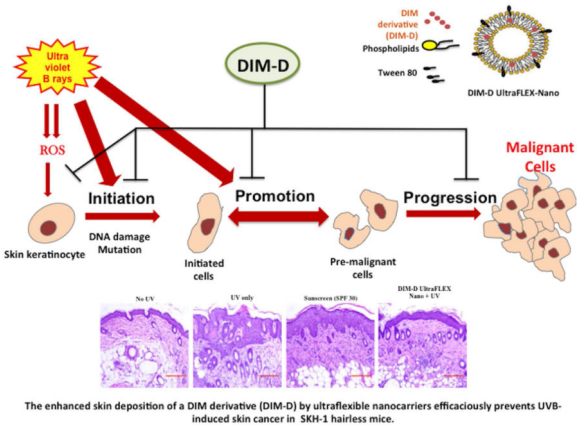

The enhanced skin deposition of a DIM derivative (DIM-D) by ultraflexible nanocarriers efficaciously prevents UVB-induced skin cancer in SKH-1 hairless mice.

Keywords

Skin delivery; Topical delivery; Skin cancer; Chemoprevention; Ultra deformable nanocarriers; Diindolymethane (DIM); Phytochemicals

1. Introduction

Ultra-flexible nanocarriers are deformable vesicles that have proven to be superior to conventional lipid nanocarriers as ideal topical delivery systems. They have demonstrated to achieve maximal therapeutic drug concentrations within the viable epidermal and dermal layers. This feature has been suggested to be due to the versatility and capability of the nanocarriers to permeate the intact skin for the deposition of their cargos into the deeper layers of the skin [1, 2]. Noteworthily, the ultra-flexible nanocarriers have been proposed to possess fluid membranes contributed to by added edge activators that render them highly elastic to squeeze through the para-cellular regions of the stratum corneum with the aid of transdermal water gradient [3]. Further, with suitable positively charged surface, these nanocarriers are able to adequately interact with and surmount the negatively charged lipid lamellae domain of the stratum corneum to enhance skin permeation efficiently. In the present study, the ultra-flexible nanocarriers were employed to potentiate the epidermal deposition of a highly lipophilic antioxidant for skin cancer chemoprevention.

Skin cancer is the most diagnosed cancer in the United States with more than 3.5 million cases of non-melanoma skin cancer (NMSC) reported annually and about 137,310 new cases projected to be diagnosed in 2015 [4]. It is caused mainly by the persistent irradiation of the skin epidermal cells by ultraviolet (UV) rays from the sun [5] although there are other important factors such as pro-carcinogenic chemicals from food and the environment that

Author Manuscript Author Manuscript Author Manuscript Author Manuscript

may also increase the risk of skin cancer [6]. Current therapies nevertheless continue to be expensive with significant scarring resulting from the surgical procedures carried out for benign tumors as well as toxic with extensive adverse effects ensuing from the long-term exposure to chemotherapies administered for metastasized cancer [7, 8].

Diverse phytochemicals have been explored for their anti-oxidative properties, their potential of inhibiting skin DNA mutagenesis as well as their slowing/reversal of the cancer initiation and progression processes [9]. Extensive research carried out on catechins from green tea, silibinin from milk thistle and proanthocyanidins from grape seeds has illustrated that these phytochemicals effectively prevent photo-carcinogenesis by inhibiting tumor incidence, reducing tumor volume and multiplicity in mice fed on their extracts [10-13]. These phytochemicals have been demonstrated to achieve this via reducing oxidative stress, DNA damage and lipid peroxidation by mopping up UV-induced reactive oxygen species (ROS) [14, 15]. However these phytochemicals have been revealed to be minimally potent, hence requiring large amounts to be administered in order to achieve therapeutic concentrations at the target sites.

In contrast, the semi-synthetic derivatives of diindolylmethane (C-DIMs), the major in vivo phytochemical derivative of indole-3-carbinol (I3C) present in cruciferous vegetables are more potent antioxidants that activate receptor-independent proapoptotic and growth inhibitory signaling pathways and suppress cancer development in skin, pancreatic, breast and prostate tissue [16-19]. Our lab has previously reported of the substantial reduction of UV-induced skin tumorigenesis by the C-DIM derivative, 1,1-bis(3’-indolyl)-1-(p-chlorophenyl) methane (DIM-D) in SKH-1 hairless mice via the initiation of apoptosis and the inhibition of ROS-induced skin lipid peroxidation, tumor incidence, epidermal hyperplasia and inflammation [14].

Nevertheless, the effective chemoprevention activity achieved depends critically on the efficiency of the delivery system utilized plus the amount of the antioxidative molecule deposited at the UV radiation targeted epidermal layer [20-23]. DIM-D has a log p value greater than 5 hence has a limitation in attaining enhanced skin delivery; in spite of the potency of a drug, the failure to attain adequate amounts at the target site restricts the therapeutic benefits that may be obtained from its application [14, 24]. Although topical drug delivery is a viable method for consideration due to its versatility and ease of drug application, efficient delivery strategies are essential to ensure that the skin barrier structure is surmounted and that therapeutic concentrations of the molecule is transported to the viable epidermal and dermal layers beneath [25-27].

Thus the objectives of the present study were 1) to develop cationic ultra-flexible nanocarriers (UltraFLEX-Nano) to encapsulate DIM-D for enhanced topical delivery, 2) to evaluate the efficacy of DIM-D-UltraFLEX-Nano for the chemoprevention of skin cancer and 3) to explore the mechanisms of chemo-preventive activity of DIM-D.

Author Manuscript Author Manuscript Author Manuscript Author Manuscript

2. Materials and Methods

2.1 Materials

The C-DIM derivative used in the study was 1,1-bis(3'-indolyl)-1-(p-chlorophenyl) methane (DIM-D) synthesized by Dr Stephen Safe's lab. Miglyol 812 and Compritol 888 ATO were kind gifts by Sasol Germany GmbH (Witten, Germany) and Gattefosse (Saint Priest, France), respectively. 1,2-dipalmitoyl-*sn*-glycero-3-phosphocholine (DPPC), 1,2-dioleoyl-3-trimethylammonium-propane (DOTAP) and 1,2-dioleoyl-*sn*-glycero-3-phosphoethanolamine (DOPE) were purchased from Avanti Polar Lipids, Inc. (Alabaster, AL, USA). Vitamin E TPGS (d-alpha tocopheryl polyethylene glycol 1000 succinate) was a kind gift from Antares Health Products, Inc. (St. Charles, Illinois, USA). Oleic acid-PEG succinimidyl glutamate ester was custom synthesized by Nanocs, Inc. (New York, NY, USA). Hydroxypropyl methylcellulose (HPMC; METHOCEL K4M Premium CR Grade) was a generous donation by DOW Chemical Company (Midland, MI, USA). RIPA lysis buffer and BCA Protein Assay Reagent Kit were purchased from G-Biosciences (Maryland Heights, MO, USA) and Pierce (Rockford, IL, USA), respectively. Polyoxyethylene-20 oleyl ether (Volpo-20) was a kind donation by Croda Inc (Edison, NJ, USA). Phosphate Buffer Saline Solution (PBS, pH 7.4) was purchased from Invitrogen. The antibodies, secondary HRP-conjugated antibodies and ABC staining immunohistochemistry (IHC) kit were purchased from Santa Cruz Biotechnology, Inc. (Santa Cruz, CA, USA). All other chemicals used in this research study were of analytical grade.

2.2 Cell line and culture

Human Embryonic Kidney cells (HEK-293) purchased from (Invitrogen; Grand Island, NY) were used for all *in vitro* experiments carried out in this study. The cells were maintained in Dulbecco's modified Eagle's medium (DMEM; Sigma-Aldrich, St Louis, MO, USA) that was supplemented with 10% fetal bovine serum (FBS) (Invitrogen; Grand Island, NY) and antibiotic-antimycotic mixture (penicillin (5000U/ml), streptomycin (0.1 mg/ml) and neomycin (0.2mg/ml) (Sigma-Aldrich; St Louis, MO)) at 37°C in the presence of 5% CO_2 and 95% relative humidity. The growth media was changed every 2 days and the cells were subcultured when 80-90% confluent with 0.25% trypsin-EDTA (Invitrogen; grand Island, NY).

2.3 Animals

SKH-1 hairless female mice (6 weeks old; Charles River Laboratories, Wilmington, MA) were used for developing the skin cancer model. The animals were housed in cages with beddings in groups (n=8) and maintained under controlled conditions of 12:12h light: dark cycle, 22 ± 2°C and 50 ± 15% RH. The mice were provided with feeding (Harlan Teklad) and water ad libitum. They were housed at Florida A&M University in accordance with the Guide for the Care and Use of Laboratory Animals and Association for Assessment and Accreditation of Laboratory Animal Care (AAALAC) and were acclimatized to laboratory conditions for a week before the onset of all experiments. The Institutional Animal Care and Use Committee (IACUC) at Florida A& M University, FL approved all animal protocols that were observed in this study.

Author Manuscript Author Manuscript Author Manuscript Author Manuscript

2.4 HPLC analysis

A Vydac reverse phase C18 (300 Å pore size silica) analytical column (5 mm, 4.6×250 mm) (GraceVydac, Columbia, MD) was used for the HPLC analysis of DIM-D with a Waters HPLC system (Waters Corp, Milford, MA). The mobile phase used consisted of an isocratic system maintained at 20% of water and 80% of acetonitrile set at a flow rate of 1.0 ml/min [14]. The amount of DIM-D present in the samples was determined at 237 nm.

2.5 Development and evaluation of Ultra-flexible nanocarriers (UltraFLEX-Nano)

2.5.1 Preparation of UltraFLEX-Nano—The nanocarriers were formulated with DPPC, DOTAP, Tween 80 and cholesterol in a weight ratio of 200:20:100:40 mg using the ethanolic injection method. The lipids and drug (20mg) were dissolved in ethanol to constitute the organic phase. Subsequently, the lipid mixture was injected in a fine stream into HPLC grade water (55°C). The mixture was continually stirred to completely evaporate off the organic solvent and the formulation was then sonicated at 30 % amplitude (Branson Digital Sonifier 450 W, Branson, USA) for 2 min to form a monodispersed nanocarriers.

2.5.2 Physicochemical characterization of UltraFLEX-Nano—The average particle size and zeta potential (ζ potential, mV) of the nanocarriers were respectively determined using Nicomp 380 ZLS (Agilent Technologies, Santa Clara, CA, USA), which employs dynamic light scattering to measure the particle size distribution and Nicomp 380 ZLS analyzer, which measures the particle electrophoretic mobility to determine the charges of the particles. All measurements were performed three times. The entrapment efficiency was determined as described earlier [28]. Briefly, the drug content was firstly determined by dissolving 100μl of the nanocarriers in ethanol to solubilize the lipids and then by diluting with a mixture of acetonitrile and water. The resulting sample was centrifuged at 10,000 rpm for 15 min and the supernatant was collected and analyzed by HPLC. Secondly, the nanocarriers were put in the donor compartment of the vivaspin centrifuge filter membrane and centrifuged at 4500 rpm for 15 min. The amount of drug present in the receiver compartment (RC) was then determined by HPLC. The entrapment efficiency was calculated using the formula:

$$\text{Entrapment efficiency } (\%) = [(\text{the total drug content} - \text{amount of drug in RC} \times 100\%)/\text{the total drug content}].$$

2.5.3 Differential Scanning Calorimetric (DSC) analysis of UltraFLEX-Nano—The DSC analysis of DIM-D-UltraFLEX-Nano was carried out using the DSCQ100 System (TA Instrument, USA) [24]. Briefly, 5 mg of the drug (crystalline), blank formulation (lyophilized) and DIM-D-UltraFLEX-Nano (lyophilized) were weighed individually into an aluminum pan (TA Instrument, USA) that was then sealed hermatically with a lid. The samples were heated at a temperature range of 30 to 180 °C with a heating rate of 5°C/min under nitrogen purge. All data was analyzed using the Universal Software analysis 2000 (TA Instrument, USA).

2.5.4 Intermittent Contact Atomic Force Microscopy (IC-AFM) of UltraFLEX-Nano—IC-AFM phase imaging of DIM-D-UltraFLEX-Nano was performed in the tapping

Author Manuscript Author Manuscript Author Manuscript Author Manuscript

mode (Bruker Nanoscope V) using the otepsa probe and was compared to the blank formulation and drug, respectively. This was done to establish the distribution of the different materials present in the samples, the phase separations as well as the drug distribution within the nanocarriers to ascertain the successful encapsulation of DIM-D within the nanocarriers. The samples were diluted (about 500x) and air-dried overnight on a microscope. All the images were obtained from a sample size equivalent to 1 μm. The measurements were carried out at room temperature (22 °C) whilst the data was analyzed using the Bruker Analysis software with the phase images overlaid on the height image.

2.6 *In vitro* skin permeation studies

2.6.1 Preparation of skin—Dermatomed human skin was used for all the permeation studies. The skin was purchased from Platinum Training (Henderson, NV), transported in 10% glycerin in saline solution with a thickness of about 0.5±0.1 mm and was stored at −80°C. The skin was defrosted and rinsed with distilled water for 15-20 min to remove excess glycerin right before all experiments. Our laboratory has previously validated the methods of storage and preparation of dermatomed human skin and has certified that the skin retains its integrity for accurate permeation results [29, 30].

2.6.2 Permeation studies with DIM-D UltraFLEX-Nano—The skin deposition of DIM-D was determined for UltraFLEX-Nano in comparison with previously optimized nanostructured lipid carriers (NLC) that had been surface-modified with oleic acid-PEG PEG succinimidyl glutamate ester (NLC-OA) and DIM-D PEG solution. DIM-D-NLC and DIM-D-NLC-OA were formulated in accordance with the protocol of Boakye et al [14]. For the permeation studies, the dermatomed human skin was mounted between the donor and receiver compartments using the Franz diffusion cells (Permegear Inc., Riegelsville, PA, USA). The receiver compartment comprised of TPGS (1%w/v), ethanol (20%v/v) and volpo (1%w/v) dissolved in PBS (pH 7.4) and was maintained at 37±0.5°C with continuous stirring at 300 rpm. About 150 μl of each formulation corresponding to 300 μg of DIM-D was applied uniformly on the entire surface of the skin (stratum corneum) in the donor compartment and the studies were carried out for 24 h under unocclusive conditions. Following the permeation studies, the leftover of each formulation was removed from the surface of the skin with a cotton swab, cleaned carefully using 50% v/v ethanol in water and then the total dosing area (0.636 cm^2) was excised using a biopsy punch. The amounts of drug retained within the skin tissue and the amount that permeated into the receiver compartment were estimated by HPLC using established methods [14].

2.6.3 Optimization, drug release and skin permeation studies of UltraFLEX-Nano matrix gel—The amount of Hydroxypropyl methylcellulose (HPMC) required for the formation of an ideal matrix gel for the nanocarriers that prevented the run-off of the dispersion from the skin surface and ensured sufficient contact-time for improved skin permeation was optimized with varying concentrations of the polymer. HPMC matrix gels containing 0.3, 1.0 and 1.5% of the polymer were prepared by dispersing the polymer in the formulation suspension, stirring continuously for a consistent gel to form and then stabilizing at room temperature for 24 hr before use. The gels were then investigated for the drug release and skin deposition of DIM-D.

Author Manuscript Author Manuscript Author Manuscript Author Manuscript

For the *in vitro* drug release studies, a semi-permeable dialysis membrane of molecular weight cut off (MWCO) of 50 kDa (Sigma Aldrich Co, MO) was used. The membrane was mounted between the donor and receiver compartments of the Franz diffusion cells as done for the skin and 150 μl of each DIM-D-UltraFLEX-Nano gel was applied to cover the entire surface of the membrane in the donor compartment. The receiver compartment was maintained as mentioned above for the skin permeation studies. At the scheduled time points, t = 0.5, 1, 2, 3, 4, 6 and 10 hr, 300 μl samples were taken from the receiver compartment and replaced with fresh buffer solution. The collected samples were then analyzed for the amount of permeated drug by HPLC. The cumulative drug release and dissolution rate constants, r_0, r_1 and r_H for zero-order, first-order and Higuchi release kinetics, respectively were estimated. Further, the exponential release rate, n was determined for Korsmeyer Peppas' release kinetics to better understand the release mechanisms of the nano gels.

The amount of DIM-D deposited within the skin tissue for each of the UltraFLEX-Nano gels was also determined using dermatomed human skin. Permeation studies were carried out for 24 hr following the protocol described above. The gel that resulted in the maximum deposition of DIM-D in the skin was selected and used for the animal studies.

2.7 Skin cancer chemoprevention studies

The UV-induced skin cancer model was developed in SKH-1 hairless female mice in accordance with the established methods of Katiyar et al [13, 31] with modifications. Briefly, the animals were divided into groups (n=8) and topically treated with DIM-D-UltraFLEX-Nano gel (300 μg of drug) daily for 5 days prior to the start of UV exposure. Following this, the animals were pretreated with DIM-D-UltraFLEX-Nano gel on alternate days (3x a week) 2 hr prior to UV irradiation (180mJ) for 6 months. The studies were carried out in comparison to a marketed sunscreen formulation (SPF 30) whilst UV-only and No UV, no drug treatment groups were employed as the negative and positive controls, respectively. The animals were irradiated from a band of UVB lamps (Daavlin, UVA/UVB Research Irradiation Unit, Bryan, OH) that was equipped with an electronic regulator for UV dosage control. The UV lamps produced UVB (290-320 nm) predominantly with less of UVA and UVC rays.

The incidence of skin tumorigenesis as well as the number of tumors formed was recorded for each animal every week for the entire duration of the chemoprevention studies. Tumors that were persistent and at least 1 mm in size were recorded. At the end of the studies, the animals were sacrificed and their dorsal skin was excised and subjected to molecular analysis.

2.8 Histology

The excised skin tissue from the *in vivo* skin cancer studies was analyzed by H&E staining and immunohistochemistry. Briefly, the skin was formalin-fixed and paraffin-embedded to obtain thin sections of the tissue. The sections were then deparaffinized, rehydrated and stained with hematoxylin with eosin employed as the counterstain.

Author Manuscript Author Manuscript Author Manuscript Author Manuscript

For the immune-histochemical studies, the paraffin-embedded skin sections were stained for 8-hydroxydeoxyguanosine (8-OHdG) protein using the protocol specified by ImmunoCruz™ mouse ABC staining kit. Briefly, the tissue sections were washed in xylene to deparaffinize and were hydrated in varying concentrations of alcohol in water. They were then incubated with the primary antibody targeting the protein of interest overnight at 4°C followed by incubation with horseradish peroxidase (HRP)-conjugated secondary antibody detecting the primary antibody. The section slides were subsequently stained with DAB chromogen and imaged using the Olympus BX40 light microscope equipped with a computer-controlled digital camera (DP71, Olympus Center Valley, PA). Positive results were considered for the brown staining of the skin sections.

2.9 Western blot analysis

Western blot analysis was carried out to estimate the expressions of critical proteins involved in the skin photocarcinogenesis. Briefly, the skin samples were homogenized in a mixture of RIPA lysis buffer, protease inhibitor (PI) and phenylmethylsulfonyl fluoride (PMSF) on ice. The protein concentration was then measured using the BCA Protein Assay Reagent Kit according to established protocol. 50 μg of the protein lysate was loaded onto a gel and subjected to SDS-polyacrylamide electrophoresis (SDS-PAGE) after which the protein bands were transferred unto membrane blots. The blots were incubated with primary antibodies for Vimentin, MMP-9, PCNA, AKT, IL10, CyclinD1, p53, p21, c-myc, TIMP1 and β-actin and detected with HRP-conjugated secondary antibodies using a SuperSignal West Pico Chemiluminescent Substrate (Pierce, Rockford, IL, USA) and BioRad ChemiDoc™ XRS+ imaging system (Hercules, CA, USA).

2.10 Statistical Analysis

All the results of the study have been expressed as the mean ± standard deviation for at least three repetitions. One-way analysis of variance (ANOVA) analysis was used for the comparison among multiple groups followed by Tukey's Multiple Comparison Test whilst student's t test analysis was used for the comparison between two groups. The mean differences were considered significant in all experiments valued at *$p < 0.05$, **$p< 0.01$ and ***$p<0.001$.

3. Results

3.1 Development and evaluation of Ultra-flexible nanocarriers (UltraFLEX-Nano)

3.1.1 Physicochemical characterization of UltraFLEX-Nano—The ultra-flexible nanocarriers formed a nanodispersion with mean particle size of 110.50±0.71 nm, polydispersity of 0.25±0.11 and zeta potential of +16.02±0.86. The estimated entrapment efficiency was 91.02±7.14%. The physicochemical characterization of the particles has been represented in supplementary table 1.

3.1.2 Differential Scanning Calorimetric (DSC) analysis of UltraFLEX-Nano—The DSC thermograms revealed the successful encapsulation of DIM-D within UltraFLEX-Nano (figure 1). The drug showed a broadened endothermic peak between 60 and 65 °C, which is consistent with prior studies carried out in our lab. However, the endothermic peak

Author Manuscript Author Manuscript Author Manuscript Author Manuscript

for the drug disappeared in the thermogram for DIM-D-UltraFLEX-Nano, suggesting that the drug was not in the free crystalline or precipitated state but in the solubilized state within the lipid-surfactant bilayers. Further, the blank formulation consisting of DPPC, DOTAP, Tween 80 and cholesterol showed a sharp endothermic peak around 155°C and two minor peaks between 160 and 170 °C. The major peak at 155°C however reduced markedly, broadened and shifted to a temperature range of 130 to 140 whilst the two minor peaks disappeared completely in the DSC thermogram for DIM-D-UltraFLEX-Nano.

3.1.3 Fourier Transform Infrared (FT-IR) spectra analysis of UltraFLEX-Nano— The FT-IR spectra of DIM-D, blank formulation and DIM-D-UltraFLEX-Nano were obtained to further confirm the encapsulation of DIM-D within UltraFLEX-Nano. The spectra have been illustrated in supplementary figure 1. The spectroscopic characterizations were carried out over the wavelength range of 4000 nm to 700 nm. The FT-IR spectra of DIM-D showed sharp peaks of medium intensity at 3409cm^{-1} (possibly due to N-H stretching vibrations of the secondary amine functional group), 1400 – 1500cm-^{1} (aromatic carbon- carbon stretching vibrations), 1035 and 1090cm^{-1} (in plane C-H bending) and 743cm^{-1} (out of plane C-H bending vibration). An additional peak of medium intensity was observed at 750 cm^{-1} possibly due to C-Cl vibration. The most notable peaks in the FI-TR spectra of the blank formulation were a broad weak band at 3300cm^{-1}(possibly due to intramolecular O-H stretching vibrations), two peaks around 2900cm^{-1} (aliphatic C-H vibration), 1730cm^{-1} (stretching vibrations of C=O) and 1468cm^{-1} (asymmetric methyl C-H bending). Nanoencapsulation of DIM-D resulted in changes along the entire wavelength range. This was observed by the appearance of new peaks, shift in peak position and changes in peak shape, slope and intensity. Quite notable amongst them was the shift in carbonyl peak of the blank liposomes shifted from 1730cm^{-1} to 1736cm^{-1}, the appearance of skeletal aromatic C-H vibration peak at 1487cm^{-1} and the appearance of a drug peak at 927cm^{-1}, which was absent in the FTIR spectra of the blank liposomes. Additionally, there was broadening of the blank liposome peaks at 1060cm^{-1} and 1090cm^{-1} upon drug encapsulation. The secondary amine peak of DIM-D was absent in the spectra of DIM-D loaded liposome. These changes could be attributed possible molecular interactions between DIM-D and the formulation components in the blank liposome.

3.1.4 Intermittent Contact Atomic Force Microscopy (IC-AFM) of UltraFLEX-Nano—IC-AFM phase imaging illustrates materials with high or low energy absorbencies to give different phase contrast images that reflect drug and material distributions [32]. To ascertain that the drug was encapsulated with the nanocarriers, the phase-contrast images were overlaid over the height-images of DIM-D, blank formulation and DIM-D-UltraFLEX-Nano (figure 2). The analysis revealed that there were notable differences between the phase images of the blank formulation and DIM-D-UltraFLEX-Nano whilst the phase image of the latter showed prominent characteristics similar to the free drug. Dark areas depict softer sample areas whilst bright areas depict relatively stiffer sample areas; the phase images of the blank formulation were darker than the phase images of DIM-D-UltraFLEX-Nano, revealing that the former was definitely softer than the latter. The phase images of the drug only were the brightest and may be attributed to the crystalline nature of the drug; this therefore accounts for the reflectively stiffer nature of DIM-D-UltraFLEX-Nano than the

Author Manuscript Author Manuscript Author Manuscript Author Manuscript

blank formulation. Also, when the particles were sectioned (data not shown), the estimated energy absorbance at the surface of the blank nanocarriers was significantly different from that of DIM-D-UltraFLEX-Nano, further revealing the presence of the drug within the latter, which modified its energy absorption features. The results hence revealed the encapsulation of DIM-D within UltraFLEX-Nano, mostly homogeneously due to the fact that the particles showed same intensity.

3.1.5 Deformability studies of UltraFLEX-Nano—The deformability of the UltraFLEX-Nano was evaluated because this feature plays a crucial role in the particles capability to squeeze through the skin pores and between the skin cells for the topical delivery of their cargos [33]. The results illustrated that UltraFLEX-Nano was more deformable and elastic than the plain Nano. The particle size of UltraFLEX-Nano before and after extrusion was ~120 and 110 nm, respectively and ~112 and 101 nm, respectively for the plain Nano. The estimated % gain of UltraFLEX-Nano after extruding through the polycarbonate membrane was approximately 95%, which was about 1.14-fold more than the plain Nano (83%) (supplementary figure 2a). Further, the deformation index (DI) for UltraFLEX-Nano was about 1.32-fold more than the plain nanocarriers. The calculated DI for UltraFLEX-Nano and plain Nano was 13.03±0.71 and 9.86±0.60, respectively (supplementary figure 2b).

3.1.6 Cell viability studies of UltraFLEX-Nano—HEK-293 cells were selected for the in vitro toxicity studies because they are commonly used to determine the safety of diverse formulated delivery systems [24]. They are embryonic kidney cells and if they can tolerate the excipients of a formulation, then it is highly probable that the formulation will not pose any toxic effects to the body cells. The results revealed that blank UltraFLEX-Nano was very well tolerated by HEK-293 cells and illustrates the relative non-toxicity of the nanocarriers (supplementary figure 2c). After 24 hr incubation of the cells with the blank formulation, there was a cell viability of 88.98±6.79% estimated at the maximum concentration of 100 %v/v.

3.2 *In vitro* skin permeation studies

3.2.1 Permeation studies with DIM-D UltraFLEX-Nano—The results of the permeation studies for DIM-D-UltraFLEX-Nano, DIM-D-NLC-OA, DIM-D-NLC and PEG solution have been represented in figure 3a. The data revealed that UltraFLEX-Nano significantly ($p<0.001$) enhanced the skin deposition of the drug by 13.83, 3.42 and 10.46-fold more than the solution, NLC-OA and NLC, respectively. This result can be attributed to the elastic and flexible nature of UltraFLEX-Nano, which allowed it to squeeze through the skin pores to enhance the permeation of DIM-D. However, no drug content was detected in the receiver compartment for any of the formulations. The calculated skin retention of DIM-D for UltraFLEX-Nano, NLC-OA, NLC and PEG solution was 99.28±6.88, 29.01±15.07, 9.49±1.55 and 7.18±0.75 μg per gram of skin, respectively.

3.2.2 Optimization, drug release and permeation studies of UltraFLEX-Nano matrix gel—The effect of HPMC polymer concentration on the release kinetics of DIM-D from UltraFLEX-Nano was studied to select the ideal system for the *in vivo* skin cancer

Author Manuscript Author Manuscript Author Manuscript Author Manuscript

studies. The cumulative drug release plots were fitted to the mathematical models for zero-order (r_0), first-order (r_1) and Higuchi-type (r_H) release kinetics in accordance with the methods of Verma et al [34] and Costa et al [35]. The slopes of the fitted plots were used to estimate the release rates. For zero-order, the cumulative % drug release (Q) was plotted against time (t); for first-order, the log of the cumulative % drug release (Ln Q) was plotted against time (t); for Higuchi-type, the cumulative % drug release (Q) was plotted against the square root of time ($\sqrt{t}$) and for Korsmeyer-Peppas type, the log of the cumulative % drug release (Ln Q) was plotted against the log of time (log t). The release studies revealed that the rate and extent of release of DIM-D was similar for all three gels with an initial burst of drug release followed by controlled-release observed for all three gels (figure 3b). Also, the release kinetics of the gels fitted suitably to the Higuchi mathematical model, which demonstrated the highest R^2 values of 0.99 to 1.00 with estimated r_H values of 9.95, 10.95 and 10.26 $hr^{-1/2}$, respectively. However, the release kinetics also fitted appropriately to Korsmeyer-Peppas with estimated release exponent values of 0.72, 0.69 and 0.69, respectively for 0.3, 1.0 1.5% gel (supplementary table 2). This revealed that the release of DIM-D from the nano gels was non-Fickian and was driven by both diffusion and polymer matrix erosion, due to the fact that the n values fell between 0.5 and 1.0.

Additionally, the permeation results revealed that the incorporation of DIM-D-UltraFLEX-Nano into HPMC matrix gel pronouncedly enhanced the skin deposition of DIM-D (supplementary figure 3a and 3b) more than the aqueous dispersion. However, the concentration of polymer played a vital role in the amount of the drug deposited within the skin layers in contrast to the release studies, which revealed similar patterns for all three gels. 0.3% HPMC gel showed the most skin deposition of DIM-D, which was about 1.04 and 2.59-fold more at the stratum corneum layer and 18.01 and 9.82-fold more at the epidermal+dermal layer than the 1.0% and 1.5% HPMC nano gels, respectively.

3.3 Skin cancer chemoprevention studies

The data collected supported previous studies that reported the chemoprevention potential of DIM-D following enhanced topical delivery [14]. Pretreatment of the SKH-1 hairless mice with DIM-D-UltraFLEX-Nano gel prior to UV exposure significantly ($p<0.05$) delayed tumorigenesis by approximately 2 weeks which was comparable to the marketed sunscreen of SPF30 (delayed tumorigenesis by 3 weeks) (figure 5). Further, the percentage of animals that showed tumors at onset of tumorigenesis for UV-only treatment was about 87.5% whilst for DIM-D-UltraFLEX-Nano and sunscreen SPF30 pretreatments, the percentages estimated were 62.5% and 37.5%, respectively (figure 4b). Also, the pretreatment of DIM-D-UltraFLEX-Nano gel significantly ($p<0.01$) reduced the average cumulative number of tumors formed by 3.3-fold more than UV-only treatment (figure 4a). At the end of 24 weeks, the recorded average numbers of tumors for the treatment groups were 20.00±2.52, 6.00±0.58 and 3.00±1.52 for UV-only, DIM-D-UltraFLEX-Nano gel and suncreen SPF 30, respectively.

3.4 Histology

The histological analysis further illustrated the chemoprevention activity of DIM-D (figure 6). DIM-D-UltraFLEX-Nano pretreatment caused pronounced decrease in UV-induced

Author Manuscript Author Manuscript Author Manuscript Author Manuscript

epidermal hyperplasia and infiltration of inflammatory cytokines into the dermis. These results were comparable to the positive control (no UV) but superior to the sunscreen (SPF 30) and the negative control (UV only), which both showed marked thickening of the stratum corneum and epidermis with extensive rete ridge elongation, which are consistent with skin tumors.

Further, pretreatment with DIM-D-UltraFLEX-Nano inhibited DNA damage as well as angiogenesis, which were evident in the reduced brown staining of 8OHdG and CD31 proteins, respectively. These results were comparable to the positive control (no UV) but markedly less than UV only treatment (negative control) (figure 6).

3.5 Western blot analysis

The western blot analysis reiterated the above chemo-preventive results of DIM-D; there were significantly ($p<0.05$) decreased expressions of PCNA, c-myc and Cyclin D1 for DIM-D-UltraFLEX-Nano pretreated groups that were comparable to the sunscreen, signifying cell cycle arrest and reduction in inflammation. There was also inhibition ($p<0.05$) of cell survival (AKT) as well as of UV-induced immunosuppression (IL10) and cell invasiveness and metastasis (MMP9 and TIMP9) by DIM-D-UltraFLEX-Nano pretreatment that was more than the sunscreen; however, the sunscreen caused greater decrease in the expression of vimentin compared to DIM-D-UltraFLEX-Nano but was determined to be not significant. Lastly, DIM-D-UltraFLEX-Nano pretreatment resulted in increased ($p<0.05$) apoptosis induction (p21 and p53), which was more than the sunscreen. The western blots and the calculated protein expressions have been represented in figures 7a and 7b, respectively.

4. Discussion

The results of the present study evidently support the effective chemoprevention activity of DIM-D resulting from its enhanced topical delivery and further illustrate some critical molecular processes intercepted by DIM-D for the prevention of UV-induced skin tumorigenesis. In this study, ultra-flexible nanocarriers were developed and evaluated for the augmented skin delivery of DIM-D for enhanced chemoprevention action due to the fact that the drug is highly lipophilic and hence has reduced permeability across the multiply-stacked bilayers of the lipid lamellae domain constituting the stratum corneum [14]. The ultra-flexible nanocarriers however have been demonstrated to be highly deformable and to possess the ability to squeeze with ease between the corneocytes of the stratum corneum to deliver their entrapped cargo into the deeper layers of the skin. This characteristic is attributed to certain single chain surfactants and phospholipids such as the tween series that cause the phospholipid bilayers of the nanocarriers to become destabilized and more elastic and flexible. [1, 36-38]. Other mechanisms proposed for their enhanced dermal delivery involve their loss of water at the uppermost relatively dehydrated skin layer that results in their shrinkage to appropriate sizes for enhanced para-cellular transport into the deeper layers of the skin, where the skin is more hydrated. Eventually, the nanocarriers become rehydrated and they recover their original sizes with which they travel farther into the skin layers to deliver their cargos [39]. This hence influenced the choice of tween 80 for the development of UltraFLEX-Nano.

Author Manuscript Author Manuscript Author Manuscript Author Manuscript

The physicochemical characteristics of the nanocarriers determined via DSC, FT-IR and AFM analyses confirmed the encapsulation of the drug within the lipid bilayers of the nanocarriers. The drug was demonstrated to be in the solubilized state, which may have contributed to the significantly ($p<0.001$) potentiated skin deposition of DIM-D by UltraFLEX-Nano in comparison to the PEG solution. Further, the data of the present study revealed that the nanocarriers were highly more deformable and flexible compared to the plain nanocarriers (without the edge activator, tween 80) and the estimated deformability index of 13.03 was comparable to previous studies [33]. Hence, the nanocarriers permeated the skin more proficiently and showed greater skin deposition of DIM-D than other nanocarriers without tween 80 incorporation; this may be accountable for the greater chemoprevention outcome exhibited for DIM-D in this study. DIM-D-UltraFLEX-Nano significantly ($p<0.05$) reduced the percentage of animals that formed tumors as well as the average number of tumors counted per treatment group at the end of the experiment compared to the negative control (UV only).

Additionally, the incorporation of UltraFLEX-Nano into a polymer matrix gel may have contributed further to the efficacy of the delivery system. Hydrogels have been illustrated to enhance the hydration and disruption of the stratum corneum as well as to form hydrophilic channels within the lipid lamellae domain, which serve as pathways for the transport of drug cargos into the skin deeper layers [14, 40, 41]. However, the amount of polymer utilized is critical to ensure that the drug is released in a timely fashion for permeation [42]. The results revealed that irrespective of the polymer concentration employed (up to 1.5%), there was a quick drug release followed by a controlled-release pattern, which is desirable for dermal drug application due to the fact that this allows for sustained therapeutic effect over prolonged periods of time. Importantly, this allows for the chemoprevention activity to be achieved over a prolonged period of time after one application compared to sunscreens, which are efficient over very short duration only.

Also, the modeling of the release kinetics revealed that the rate of drug release from the matrices may have been caused by both drug diffusion from UltraFLEX-Nano and HPMC polymer chain relaxation/erosion mechanisms, which is in agreement with the studies of Verma et al who have illustrated that for swellable systems, the diffusion and polymeric chain relaxation rates are critical factors that affect drug release rates. The authors showed that when the polymer relaxation rate was similar to that of the diffusion, the anomalous or non-Fickian diffusion pattern of drug release was observed [34]. However, there was reduced deposition of DIM-D within the skin layers observed with increase in polymer concentration, suggesting that there may be other factors playing roles in the permeation of the drug, which is highly lipophilic such as polymer relaxation with time, polymer interaction with the drug and drug permeation with time. Also, increase in polymer concentration tends to increase viscosity of the aqueous formulation, which may also have an impact on the release rate of the drug and the extent of permeation into the skin.

Noteworthily, the augmented dermal delivery of DIM-D efficaciously interrupted the complex cascade of events responsible for the UV-induced skin oxidative damage and tumorigenesis. Pretreatment of the animals with DIM-D-UltraFLEX-Nano prominently reduced DNA damage, which is generally triggered by persistent UV irradiation and is

Author Manuscript Author Manuscript Author Manuscript Author Manuscript

critical for the initiation of the mutagenic process if not repaired properly [43]. This was evident in the pronounced reduction in expression of 8-hyrdoxy deoxyguanosine (8OHdG). Various studies have illustrated that the persistent irradiation causes the depletion of glutathione and results subsequently in the accumulation of reactive oxygen species that produce lipid peroxidation and DNA damage [13, 44-46]. This result is consequently in agreement with previous data that demonstrated the anti-oxidative potency of DIM-D by alleviating lipid peroxidation and protein carbonylation and hence suggested its prospective use for chemoprevention activity against skin cancer [5].

Further, DIM-D-UltraFLEX-Nano significantly reduced UV-induced inflammation that precedes tumor formation. This usually corresponds with increased keratinocyte hyper proliferation and is accounts for the erythema and epidermal hyperplasia that is observed with the UV-regulated carcinogenic process. Importantly, the data revealed that DIM-D-UltraFLEX-Nano delayed and reduced skin tumorigenesis that was comparable to the sunscreen; however, the role of sunscreen in skin cancer chemoprevention varies from that of DIM-D. Sunscreens have been indicated to serve as a protective barrier for the skin by obstructing the penetration of UV rays into the epidermal and dermal layers via direct absorption of the rays or via reflection and scattering of the rays [47, 48]. However, the involvements of sunscreens in preventing some of the molecular events that are initiated within the UV irradiated skin cells remain fairly researched. This fact became apparent in the western blot and histological analysis, which illustrated that DIM-D-UltraFLEX-Nano inhibited epidermal hyperplasia and cell proliferation (AKT, PCNA, cyclin D1 and c-myc) more effectively than the sunscreen.

Importantly, DIM-D-UltraFLEX-Nano caused greater induction of apoptosis compared to the sunscreen, which is vital because the chronic UV-irradiated skin cells tend to become apoptosis-resistant with increased cell survival due to p53 mutations that are induced and is important for the sustenance and progression of the cells to malignancy [49, 50]. This enables the premalignant cells to achieve a growth advantage to hyper proliferate and to establish a colony of cancer cells [50]. These results support the report of Boakye et al that revealed that DIM-D pretreatment of SKH-1 mice prior to UV irradiation resulted in increased expressions of pro-apoptotic proteins with corresponding decrease in skin inflammation [14]. Research has indicated that apoptosis induction is crucial in premalignant skin cells to ensure that the cells do not progress to the tumor stage [13].

Additionally, DIM-D-UltraFLEX-Nano pretreatment inhibited cell cycle progression and survival as well as the epithelial-to-mesenchymal transition, which usually results in more aggressive and metastatic morphology of the pre-malignant skin cells [51]. This was revealed in the significant ($p<0.05$) reduction of MMP9 and vimentin with consequent increase in TIMP1 by DIM-D-UltraFLEX-Nano. Recent studies have shown that the C-DIMs exhibit potent inhibitory effects in bladder, lung and breast cancers by stimulating cell cycle arrest and reduction in metastasis [52, 53]. Also, the suppression of the skin immune system triggered by UV radiation, which is responsible for DNA damage and skin mutagenesis [54] was inhibited by DIM-D-UltraFLEX-Nano; the results revealed that the drug significantly ($p<0.05$) reduced the activation of IL10 more than the sunscreen. Skin immunosuppression is a critical step and results from UV-induced damage to the Langerhans

Author Manuscript Author Manuscript Author Manuscript Author Manuscript

cells or from the activation of inflammatory macrophages, which leads to the recruitment of suppressor T cells [55]. Other studies have also indicated the activation of cytokines such as IL10 and TNFα, which prevent the activation of T-cells for immune responses that are released by the keratinocytes following UV damage [56]. Hence, although the sunscreen showed slightly better chemopreventive activity in inhibiting skin cancer, DIM-D-UltraFLEX-Nano is a viable alternate for consideration for chemoprevention due to its interception of the molecular cascades, possibly for combination therapy with sunscreens to increase the efficacy of skin cancer chemoprevention.

5. Conclusion

Overall, UltraFLEX-Nano was more efficient in surmounting the skin barrier function for the enhanced topical delivery of DIM-D compared to the PEG solution. The enhanced skin delivery of DIM-D resulted in efficacious inhibition of skin carcinogenesis, which was almost comparable to sunscreen (SPF30). Further, DIM-D potently reduced the number of tumors induced by the UV radiation as well as the number of animals that showed tumors at the onset of tumor formation. DIM-D exhibited its chemoprevention activities via induction of apoptosis, arrest of cell cycle and inhibition of keratinocyte proliferation.

Supplementary Material

Refer to Web version on PubMed Central for supplementary material.

Acknowledgements

The authors would want to extend their gratitude to Dr. Gautam Behl of the Department of Pharmaceutics, Florida A & M University and to Dr Eric Lochner of the Department of Physics, Florida State University, Tallahassee, FL for their enormous guidance and contribution to this project.

This project was supported by the National Center for Research Resources and the National Institute of Minority Health and Health Disparities of the National Institutes of Health [Grant Number 8 G12 MD007582-28 and 2 G12 RR003020]

References

1. Cevc G, et al. Ultraflexible vesicles, Transfersomes, have an extremely low pore penetration resistance and transport therapeutic amounts of insulin across the intact mammalian skin. Biochim Biophys Acta. 1998; 1368(2):201–15. [PubMed: 9459598]
2. Cevc G. Transfersomes, liposomes and other lipid suspensions on the skin: permeation enhancement, vesicle penetration, and transdermal drug delivery. Crit Rev Ther Drug Carrier Syst. 1996; 13(3-4):257–388. [PubMed: 9016383]
3. Kim A, et al. In vitro and in vivo transfection efficiency of a novel ultradeformable cationic liposome. Biomaterials. 2004; 25(2):305–13. [PubMed: 14585718]
4. Rogers HW, et al. Incidence estimate of nonmelanoma skin cancer in the United States, 2006. Arch Dermatol. 2010; 146(3):283–7. [PubMed: 20231499]
5. Boakye CH, et al. Chemoprevention of skin cancer with 1,1-Bis (3'-indolyl)-1-(aromatic) methane analog through induction of the orphan nuclear receptor, NR4A2 (Nurr1). PLoS One. 2013; 8(8):e69519. [PubMed: 23950896]
6. Canene-Adams K, et al. Dietary chemoprevention of PhIP induced carcinogenesis in male Fischer 344 rats with tomato and broccoli. PLoS One. 2013; 8(11):e79842. [PubMed: 24312188]

Author Manuscript Author Manuscript Author Manuscript Author Manuscript

7. Das M, Mohanty C, Sahoo SK. Ligand-based targeted therapy for cancer tissue. Expert Opin Drug Deliv. 2009; 6(3):285–304. [PubMed: 19327045]
8. Sahoo SK, Labhasetwar V. Nanotech approaches to drug delivery and imaging. Drug Discov Today. 2003; 8(24):1112–20. [PubMed: 14678737]
9. Pathak N, et al. Cancer chemopreventive effects of the flavonoid-rich fraction isolated from papaya seeds. Nutr Cancer. 2014; 66(5):857–71. [PubMed: 24820939]
10. Mittal A, Elmets CA, Katiyar SK. Dietary feeding of proanthocyanidins from grape seeds prevents photocarcinogenesis in SKH-1 hairless mice: relationship to decreased fat and lipid peroxidation. Carcinogenesis. 2003; 24(8):1379–88. [PubMed: 12807737]
11. Mittal A, et al. Exceptionally high protection of photocarcinogenesis by topical application of (--)-epigallocatechin-3-gallate in hydrophilic cream in SKH-1 hairless mouse model: relationship to inhibition of UVB-induced global DNA hypomethylation. Neoplasia. 2003; 5(6):555–65. [PubMed: 14965448]
12. Sharma SD, Katiyar SK. Dietary grape seed proanthocyanidins inhibit UVB-induced cyclooxygenase-2 expression and other inflammatory mediators in UVB-exposed skin and skin tumors of SKH-1 hairless mice. Pharm Res. 2010; 27(6):1092–102. [PubMed: 20143255]
13. Katiyar SK, Mantena SK, Meeran SM. Silymarin protects epidermal keratinocytes from ultraviolet radiation-induced apoptosis and DNA damage by nucleotide excision repair mechanism. PLoS One. 2011; 6(6):e21410. [PubMed: 21731736]
14. Boakye CH, et al. Enhanced Percutaneous Delivery of 1, 1-bis (3-indolyl)-1-(p-chlorophenyl) Methane for Skin Cancer Chemoprevention. Journal of Biomedical Nanotechnology. 2015; 11(7): 1269–1281. [PubMed: 26307849]
15. Ali H, et al. Isolation and evaluation of anticancer efficacy of stigmasterol in a mouse model of DMBA-induced skin carcinoma. Drug Des Devel Ther. 2015; 9:2793–800.
16. Rahimi M, Huang K-L, Tang CK. 3, 3'-Diindolylmethane (DIM) inhibits the growth and invasion of drug-resistant human cancer cells expressing EGFR mutants. Cancer letters. 2010; 295(1):59–68. [PubMed: 20299148]
17. Lee SH, et al. Indole-3-carbinol and 3,3'-diindolylmethane induce expression of NAG-1 in a p53-independent manner. Biochem Biophys Res Commun. 2005; 328(1):63–9. [PubMed: 15670751]
18. Banerjee S, et al. Attenuation of multi-targeted proliferation-linked signaling by 3,3'-diindolylmethane (DIM): from bench to clinic. Mutat Res. 2011; 728(1-2):47–66. [PubMed: 21703360]
19. Azmi AS, et al. Chemoprevention of pancreatic cancer: characterization of Par-4 and its modulation by 3,3' diindolylmethane (DIM). Pharm Res. 2008; 25(9):2117–24. [PubMed: 18427961]
20. Maeda H, Sawa T, Konno T. Mechanism of tumor-targeted delivery of macromolecular drugs, including the EPR effect in solid tumor and clinical overview of the prototype polymeric drug SMANCS. J Control Release. 2001; 74(1-3):47–61. [PubMed: 11489482]
21. Labiris NR, Dolovich MB. Pulmonary drug delivery. Part II: the role of inhalant delivery devices and drug formulations in therapeutic effectiveness of aerosolized medications. Br J Clin Pharmacol. 2003; 56(6):600–12. [PubMed: 14616419]
22. Mitragotri S, et al. A mechanistic study of ultrasonically-enhanced transdermal drug delivery. J Pharm Sci. 1995; 84(6):697–706. [PubMed: 7562407]
23. Jang SH, et al. Drug delivery and transport to solid tumors. Pharm Res. 2003; 20(9):1337–50. [PubMed: 14567626]
24. Marepally S, et al. Topical administration of dual siRNAs using fusogenic lipid nanoparticles for treating psoriatic-like plaques. Nanomedicine. 2014; 9(14):2157–2174. [PubMed: 24593003]
25. Barry BW. Novel mechanisms and devices to enable successful transdermal drug delivery. Eur J Pharm Sci. 2001; 14(2):101–14. [PubMed: 11500256]
26. Kumar S, et al. Peptides as skin penetration enhancers: mechanisms of action. J Control Release. 2015; 199:168–78. [PubMed: 25499919]
27. Shah PP, Desai PR, Singh M. Effect of oleic acid modified polymeric bilayered nanoparticles on percutaneous delivery of spantide II and ketoprofen. J Control Release. 2012; 158(2):336–45. [PubMed: 22134117]

Author Manuscript Author Manuscript Author Manuscript Author Manuscript

28. Patlolla RR, et al. Translocation of cell penetrating peptide engrafted nanoparticles across skin layers. Biomaterials. 2010; 31(21):5598–607. [PubMed: 20413152]
29. Shah PP, et al. Enhanced skin permeation using polyarginine modified nanostructured lipid carriers. Journal of Controlled Release. 2012; 161(3):735–745. [PubMed: 22617521]
30. Marepally, S., et al. Design, synthesis of novel lipids as chemical permeation enhancers and development of nanoparticle system for transdermal drug delivery.. 2013.
31. Vaid M, Sharma SD, Katiyar SK. Honokiol, a phytochemical from the Magnolia plant, inhibits photocarcinogenesis by targeting UVB-induced inflammatory mediators and cell cycle regulators: development of topical formulation. Carcinogenesis. 2010; 31(11):2004–11. [PubMed: 20823108]
32. Sitterberg J, et al. Utilising atomic force microscopy for the characterisation of nanoscale drug delivery systems. Eur J Pharm Biopharm. 2010; 74(1):2–13. [PubMed: 19755155]
33. Manca ML, et al. Glycerosomes: a new tool for effective dermal and transdermal drug delivery. Int J Pharm. 2013; 455(1-2):66–74. [PubMed: 23911913]
34. Prasad Verma PR, Chandak AR. Development of matrix controlled transdermal delivery systems of pentazocine: In vitro/in vivo performance. Acta Pharm. 2009; 59(2):171–86. [PubMed: 19564142]
35. Costa P, Sousa Lobo JM. Modeling and comparison of dissolution profiles. Eur J Pharm Sci. 2001; 13(2):123–33. [PubMed: 11297896]
36. Gupta PN, et al. Non-invasive vaccine delivery in transfersomes, niosomes and liposomes: a comparative study. Int J Pharm. 2005; 293(1-2):73–82. [PubMed: 15778046]
37. Cosco D, et al. Ultradeformable liposomes as multidrug carrier of resveratrol and 5-fluorouracil for their topical delivery. Int J Pharm. 2015; 489(1-2):1–10. [PubMed: 25899287]
38. Priyanka K, Singh S. A review on skin targeted delivery of bioactives as ultradeformable vesicles: overcoming the penetration problem. Curr Drug Targets. 2014; 15(2):184–98. [PubMed: 24410447]
39. Schatzlein A, Cevc G. Non-uniform cellular packing of the stratum corneum and permeability barrier function of intact skin: a high-resolution confocal laser scanning microscopy study using highly deformable vesicles (Transfersomes). Br J Dermatol. 1998; 138(4):583–92. [PubMed: 9640361]
40. Desai P, Patlolla RR, Singh M. Interaction of nanoparticles and cel-penetrating peptides with skin for transdermal drug delivery. Molecular membrane biology. 2010; 27(7):247–259. [PubMed: 21028936]
41. Uner M, et al. Skin moisturizing effect and skin penetration of ascorbyl palmitate entrapped in solid lipid nanoparticles (SLN) and nanostructured lipid carriers (NLC) incorporated into hydrogel. Pharmazie. 2005; 60(10):751–5. [PubMed: 16259122]
42. Shah PP, et al. Skin permeating nanogel for the cutaneous co-delivery of two anti-inflammatory drugs. Biomaterials. 2012; 33(5):1607–17. [PubMed: 22118820]
43. Moriwaki S. Hereditary Disorders with Defective Repair of UV-Induced DNA Damage. Jpn Clin Med. 2013; 4:29–35. [PubMed: 23966815]
44. Melis JP, et al. Slow accumulation of mutations in Xpc-/- mice upon induction of oxidative stress. DNA Repair (Amst). 2013; 12(12):1081–6. [PubMed: 24084170]
45. Parihar A, et al. Importance of cytochrome c redox state for ceramide-induced apoptosis of human mammary adenocarcinoma cells. Biochim Biophys Acta. 2010; 1800(7):646–54. [PubMed: 20382204]
46. Ismail AM, et al. Extra virgin olive oil potentiates the effects of aromatase inhibitors via glutathione depletion in estrogen receptor-positive human breast cancer (MCF-7) cells. Food Chem Toxicol. 2013; 62:817–24. [PubMed: 24161488]
47. Baker LA, et al. Probing the Ultrafast Energy Dissipation Mechanism of the Sunscreen Oxybenzone after UVA Irradiation. J Phys Chem Lett. 2015; 6(8):1363–8. [PubMed: 26263136]
48. Gasparro FP. Sunscreens, skin photobiology, and skin cancer: the need for UVA protection and evaluation of efficacy. Environ Health Perspect. 2000; 108(Suppl 1):71–8. [PubMed: 10698724]
49. Carr TD, et al. Inhibition of mTOR suppresses UVB-induced keratinocyte proliferation and survival. Cancer Prev Res (Phila). 2012; 5(12):1394–404. [PubMed: 23129577]

Author Manuscript Author Manuscript Author Manuscript Author Manuscript

50. Jonason AS, et al. Frequent clones of p53-mutated keratinocytes in normal human skin. Proc Natl Acad Sci U S A. 1996; 93(24):14025–9. [PubMed: 8943054]

51. Singh M, Suman S, Shukla Y. New Enlightenment of Skin Cancer Chemoprevention through Phytochemicals: In Vitro and In Vivo Studies and the Underlying Mechanisms. Biomed Res Int. 2014; 2014:243452. [PubMed: 24757666]

52. Inamoto T, et al. 1, 1-Bis (3'-indolyl)-1-(p-chlorophenyl) methane activates the orphan nuclear receptor Nurr1 and inhibits bladder cancer growth. Molecular cancer therapeutics. 2008; 7(12): 3825–3833. [PubMed: 19074857]

53. Andey T, et al. 1,1-Bis (3'-indolyl)-1-(p-substitutedphenyl)methane compounds inhibit lung cancer cell and tumor growth in a metastasis model. Eur J Pharm Sci. 2013; 50(2):227–41. [PubMed: 23892137]

54. Schwarz T. [Ultraviolet radiation--immune response]. J Dtsch Dermatol Ges. 2005; 3(Suppl 2):S11–8. [PubMed: 16117738]

55. Kripke ML. Immunological effects of ultraviolet radiation. J Dermatol. 1991; 18(8):429–33. [PubMed: 1761789]

56. Ullrich SE. Modulation of immunity by ultraviolet radiation: key effects on antigen presentation. J Invest Dermatol. 1995; 105(1 Suppl):30S–36S. [PubMed: 7615994]

Author Manuscript Author Manuscript Author Manuscript Author Manuscript

Highlights

- The ultra-flexible nanocarriers are highly permeable across the stratum corneum.
- DIM-D-ultra-FLEX-Nano delayed UV-induced skin tumorigenesis and tumor multiplicity.
- It decreased DNA damage, skin inflammation, epidermal hyperplasia and cell survival.

Author Manuscript Author Manuscript Author Manuscript Author Manuscript

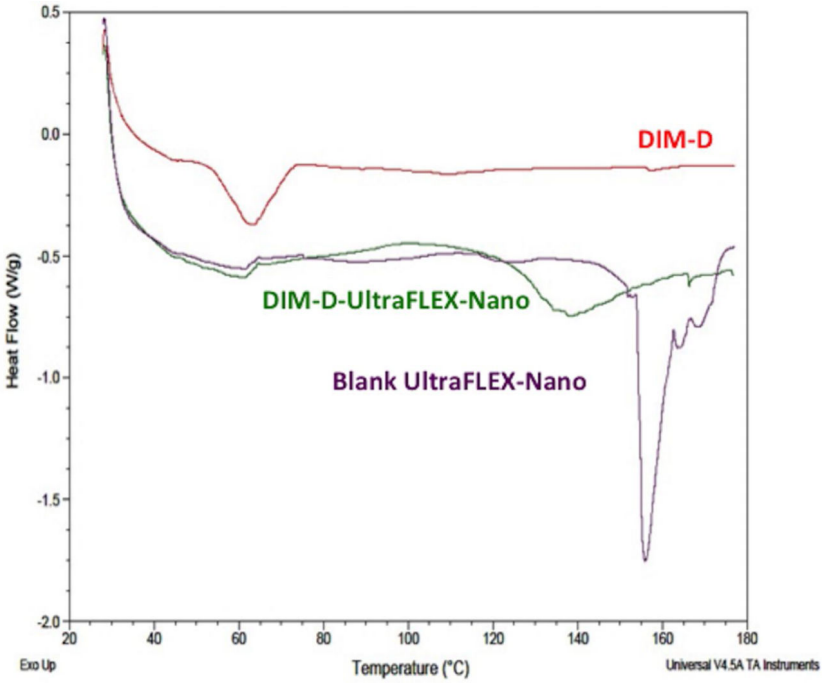

Figure 1.
Differential scanning calorimetric analysis showing the encapsulation of DIM-D in UltraFLEX-Nano.

Author Manuscript Author Manuscript Author Manuscript Author Manuscript

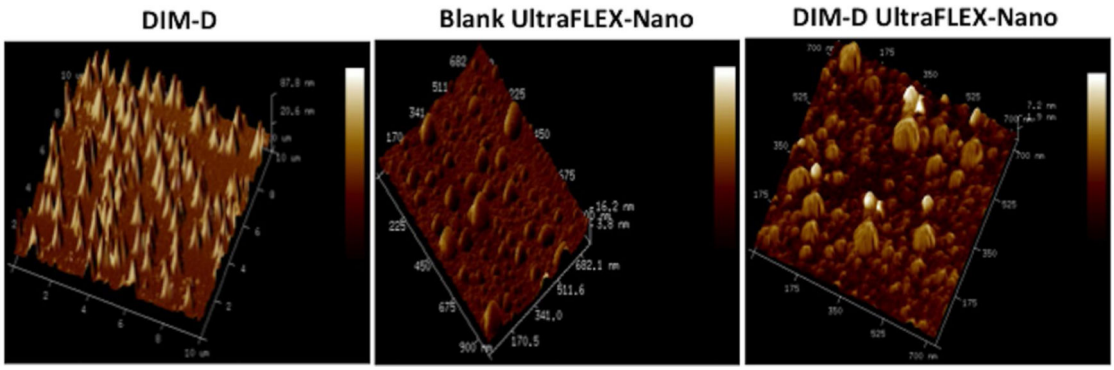

Figure 2.

Atomic Force Microscopic (AFM) phase imaging of DIM-D, blank UltraFLEX-Nano and DIM-D-UltraFLEX-Nano. Dark areas represent soft materials whilst brighter areas are relatively harder. The results show the presence of DIM-D within the nanocarriers.

Author Manuscript Author Manuscript Author Manuscript Author Manuscript

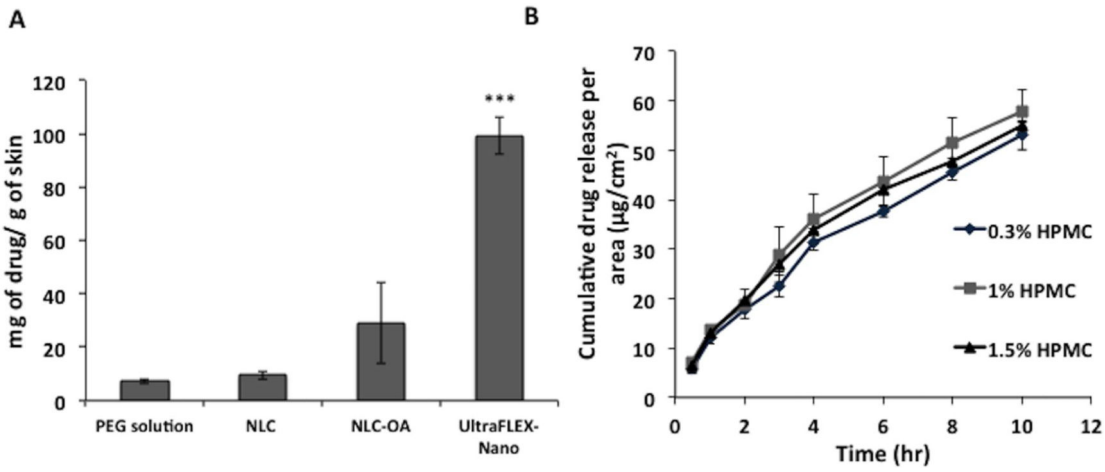

Figure 3.

A) Skin deposition of DIM-D by UltraFLEX-Nano in comparison to PEG solution, NLC-OA and NLC in dermatomed human skin after 24 hr. B) Drug release profiles of 0.3, 1.0 ad 1.5% DIM-D-UltraFLEX-Nano HPMC gels. Data has been represented as the mean ± SD. ***p<0.001.

Author Manuscript Author Manuscript Author Manuscript Author Manuscript

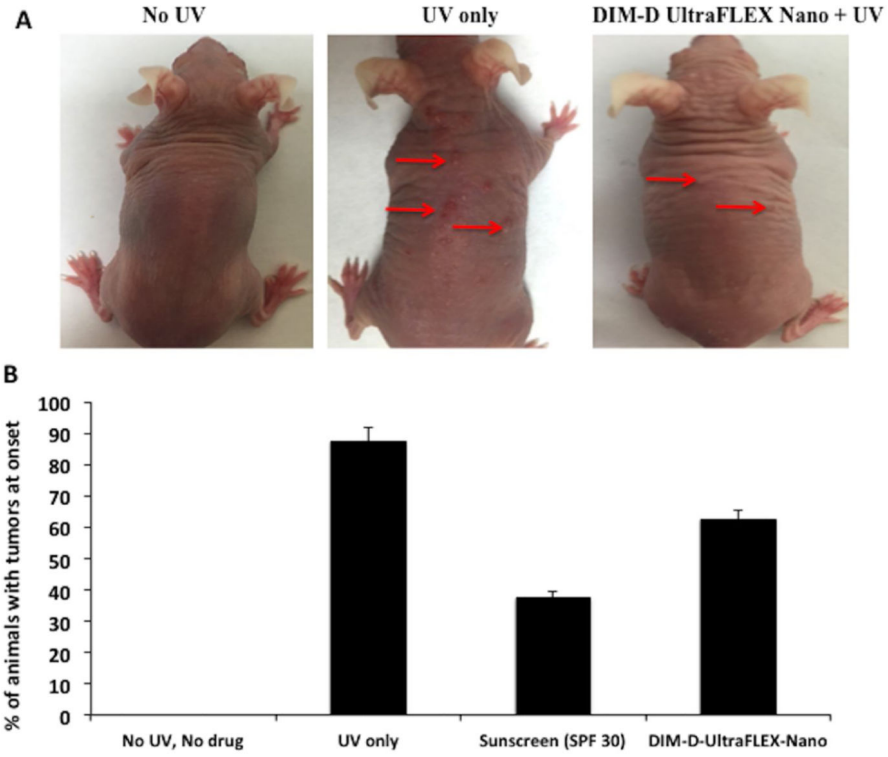

Figure 4.

A) Pictures of dorsal regions of SKH-1 hairless mice showing the tumors formed with UV only irradiation in comparison to pretreatment with DIM-D-UltraFLEX-Nano and sunscreen (SPF30). B) Representation of percentage of animals showing tumors at the onset of tumorigenesis.

Author Manuscript Author Manuscript Author Manuscript Author Manuscript

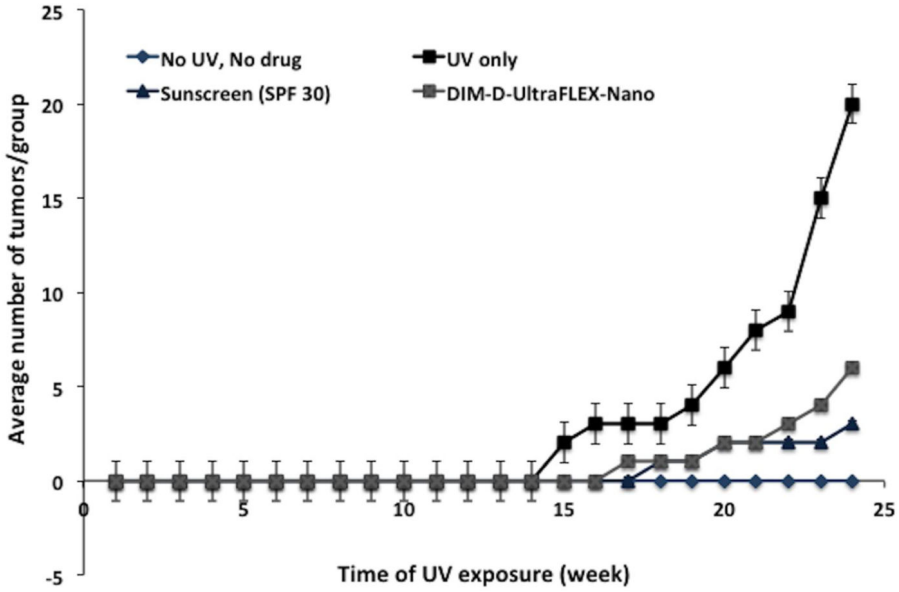

Figure 5.

Representation of the average number of tumors formed per group and the time of tumorigenesis initiation during UV exposure.

Author Manuscript Author Manuscript Author Manuscript Author Manuscript

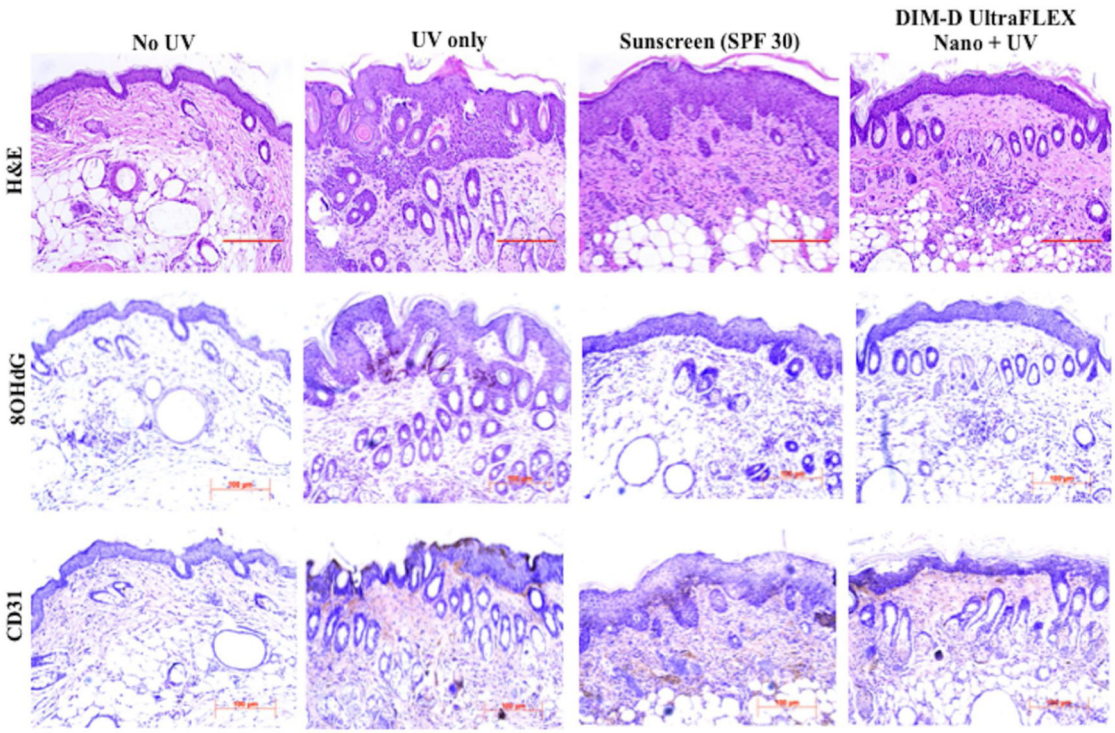

Figure 6.

Histological analysis of skin after UV experiment showing H&E staining and staining of 8OHdG and CD31 markers. Brown stain is indicative of positive results for the proteins.

Author Manuscript Author Manuscript Author Manuscript Author Manuscript

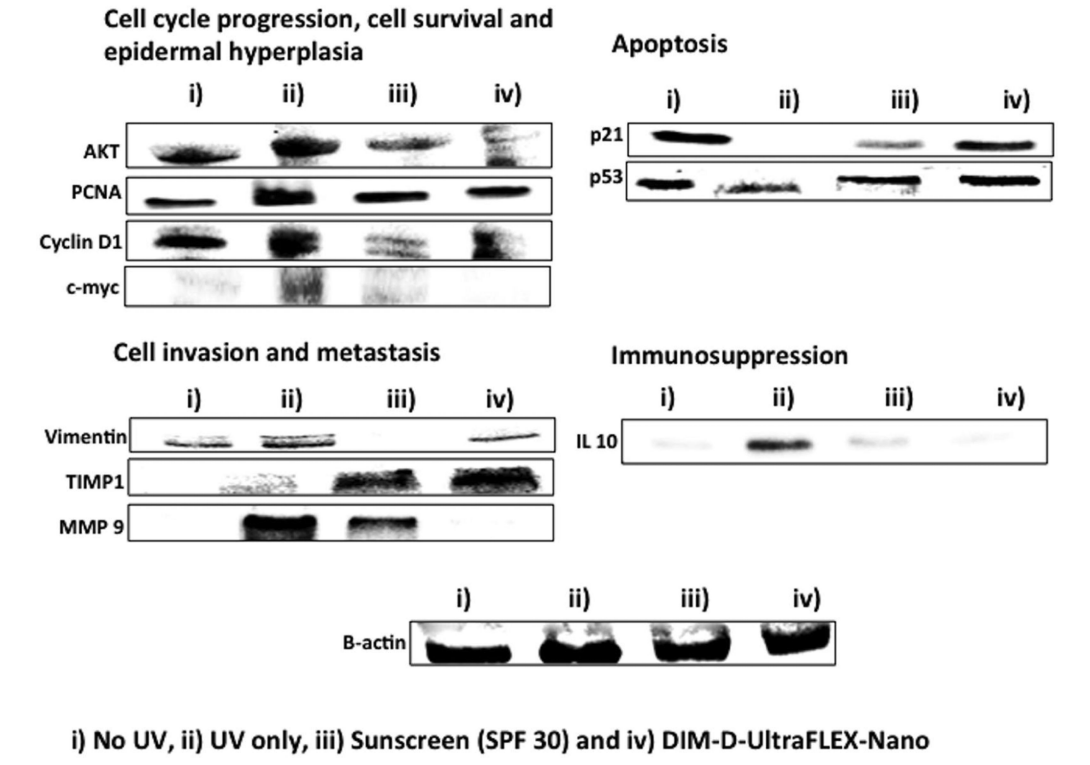

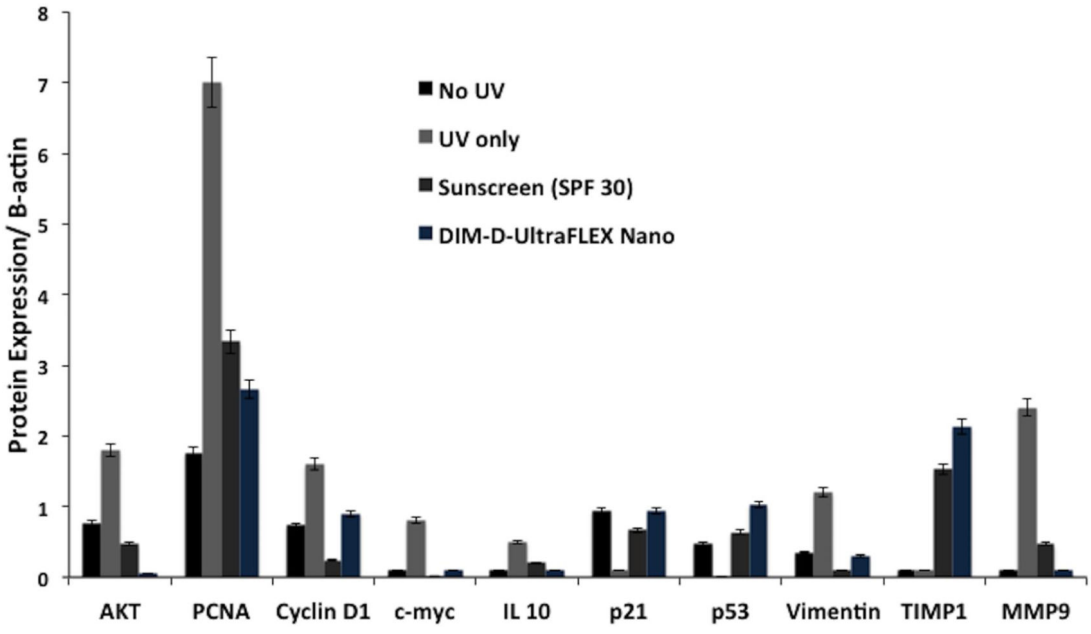

Figure 7.

Western blot analysis of skin after UV experiment showing A) protein bands and B) quantified protein expressions for the different proteins. Data has been represented as the mean ± SD. *p<0.05, **p<0.01 and ***p<0.001.